Long-Lived Photoinduced Charges in Donor−Acceptor Anthraquinone-Substituted Thiophene Copolymers

Silvia Luzzati,*,† Markus Scharber,‡,§ Marinella Catellani,† Francesco Giacalone,|| José L. Segura,|| Nazario Martin,|| Helmut Neugebauer,‡ and N. Serdar Sariciftci‡

Istituto per lo Studio delle Macromolecole, Consiglio Nazionale delle Ricerche, Via Bassini 15, I-20133 Milano, Italy, Linz Institute for Organic Solar Cells (LIOS), Physical Chemistry, Johannes Kepler University Linz, Altenbergerstrasse 69, A-4040 Linz, Austria, and Departamento de Química Orgánica, Universidad Complutense, 28040 Madrid, Spain

Received: November 9, 2005; In Final Form: January 23, 2006

The photoinduced charge-transfer properties of a series of polyalkylthiophene copolymers, carrying anthraquinone substituents covalently linked to the conjugated backbone, have been studied in the solid state by photoinduced absorption (PA) and light-induced electron spin resonance (LESR) spectroscopy. The measurements indicate the formation of metastable charges arising from the photoinduced electron transfer from the polythiophene backbone to the anthraquinone moieties. At low temperatures (below 200 K), long-lived persistent charges are formed, exhibiting lifetimes that extend for several minutes; their recombination kinetics has been studied by following the formation and decay of the PA and LESR signals. The results are rationalized using a model originally proposed to describe the low-temperature recombination kinetics of long-lived photoexcited carriers in amorphous inorganic semiconductors. It is clearly evidenced that, in these polymers, the number of acceptor substituents in the chain, easily tuned by chemical tailoring, plays a key role in the photoexcitation scenario.

Introduction

Conjugated polymers have been the subject of a large number of academic and industrial studies in the past decades because of their potential applications in organic electronics. Among the various applications, polymeric materials have been considered for the fabrication of low-cost photoelectric conversion devices such as photodetectors or solar cells.[1,2]

The charge photogeneration in conjugated polymers is intrinsically poor, as the photoabsorption creates electron−hole pairs that are bound in excitons. Their dissociation, induced by a charge transfer between materials with different ionization potentials and electron affinities, enhances the photoconductive response of the material, opening up to polymeric photovoltaic applications. The discovery of an efficient photoinduced charge separation between conducting polymers, acting as donors, and fullerene and its derivatives, as acceptors,[3,4] triggered numerous investigations in this field, spanning from the search for new donor/acceptor systems to the optimization of the device architecture.

The assessment, by photophysical studies, of the photoinduced charge-transfer process of polymer/acceptor composite films is of fundamental interest for both material characterization and device fabrication. In particular, the formation of long-lived metastable charged states, arising from a fast electron transfer from the electron-donating conjugated backbone to the acceptors, is a prerequisite for the photogeneration of free carriers. These features are fulfilled in conjugated polymer/fullerene blends, where the kinetics of the photoinduced charge-transfer process has been studied in detail: the charge separation occurs on a 10-fs time scale after photoexcitation,[5] and the back transfer occurs on the order of microseconds at room temperature.[6] At lower temperatures, the charge-separated states are living longer (milliseconds at 80 K)[7] and persistent charge carriers, with recombination lifetimes that extend over several minutes or hours, have also been observed.[8,9] The recombination mechanism of these persistent charges[9] has features common to disordered inorganic materials, such as hydrogenated amorphous silicon and germanium.[10] It has been suggested that, in polymer/fullerene blends, the charge trapping at lower temperatures is not related to specific polymer impurities and defects but is intrinsic to disordered organic and inorganic materials.[9]

The most promising polymeric photovoltaic device architecture is the bulk heterojunction, in which the electron-donor polymer is blended with acceptor molecules (i.e., fullerenes[11]) or polymers.[12] The tendency for phase segregation of the donor and acceptor components has a crucial role in device efficiencies,[13] so that much effort has been devoted to the optimization of the morphology of the photoactive blend. One of the proposed approaches to attain control of the morphology of the donor−acceptor phases is to design macromolecules in which the donor and acceptor moieities are chemically linked. Systems such as diblock copolymers have been synthesized.[14,15] Moreover the covalent linking of electron-accepting moieties to a hole-transporting conjugated polymer backbone has also been proposed. These macromolecules have, in principle, two different pathways ("cables") for different signs of charges, so they have been viewed ideally as "double cables" in which a balanced transport of electrons and holes can be achieved.[16] Different types of conjugated polymers bearing side chains containing

* To whom correspondence should be addressed. E-mail: silvia.luzzati@ismac.cnr.it.

† Consiglio Nazionale delle Ricerche

‡ Johannes Kepler University.

§ Present address: Konarka Austria, Forschungs- und Entwicklungs GmbH, Gruberstrasse 40-42, A-4020 Linz, Austria.

|| Universidad Complutense.

10.1021/jp056483g CCC: $33.50
Published on Web 03/01/2006

CHART 1: Chemical Structure of the PTAs

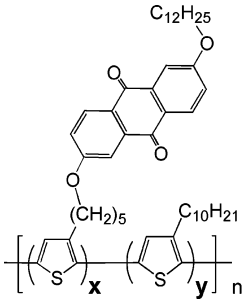

PTA100 x = 100 %
PTA75 x = 75 %, y = 25 %
PTA50 x = 50 %, y = 50 %
PTA25 x = 25 %, y = 75 %
PDT y = 100 %

acceptors such as fullerene derivatives,[17−19] tetracyanoanthraquinodimethane,[20,21] perylenes,[22] and phthalocyanines[23] have been synthesized. One of the major issues arising from these studies is the need to obtain processable polymers with high contents of acceptor substituents.

Within this approach, we have prepared a series of polythiophene copolymers containing, in the backbone, alkylthiophene units and thiophene rings with anthraquinone acceptor moieties in the alkyl side chain.[24] The peculiar feature of these materials is that the content of acceptor can be easily tuned and even 100% anthraquinone substitution leads to a soluble polymer.

Following the initial report showing the occurrence of a photoinduced electron transfer from the polythiophene backbone to the anthraquinone acceptor moieties,[25] in this work, a more detailed photophysical characterization is presented. The kinetics of persistent photogenerated charges, observed below 200 K, is studied by following the formation and decay of the photoinduced absorption (PA) and light-induced electron spin resonance (LESR) signals.

Experimental Section

The copolymers, containing decylthiophenes and anthraquinone-substituted thiophene monomers, were prepared by chemical oxidative coupling with $FeCl_3$. We synthesized a polymer with all of the thiophene rings substituted with anthraquinone and three copolymers with 25%, 50%, and 75% of the units containing acceptor molecules (herein PTA100, PTA25, PTA50, and PTA75, respectively); their chemical structures are reported in Chart 1. The macromolecular characterization indicates that the random copolymers contain the same comonomer ratio as the monomer feed at the start of polymerization.[24] A polydecylthiophene (PDT) obtained by the same synthetic route, with a similar degree of regioregularity, was used for comparison.

The samples for the photoinduced absorption (PA) measurements were prepared by drop casting from solutions on KBr windows. The film thickness of the different copolymers was adjusted to obtain similar absorbances at the laser excitation wavelength (OD of 1.7 at 514 nm). The samples were kept in a variable-temperature cryostat allowing measurements in the range 78−300 K.

The PA spectra were measured with an FTIR spectrometer covering a spectral range from 0.05 to 1.8 eV. The fractional changes in transmission were measured in response to an incident laser line at 514 nm by the subsequent accumulation of scans with laser on and laser off. The on/off modulation was driven by a mechanical shutter with frequencies varying from 0.5 to 0.0141 Hz. The kinetics was studied according to the following experimental procedure: (1) Cool the sample to 78 K in darkness. (2) Perform a scan to use as a reference. (3) Turn on the laser excitation and record scans under illumination every 0.3 s for 200−300 s. (4) Switch off the laser excitation and warm the sample to room temperature for 1 h before starting to cool it again to the working temperature. The annealing to room temperature is necessary to eliminate the persistent signal completely. The decays were measured by a similar procedure, with the scans recorded in darkness instead of under illumination, after 3 min of laser exposure.

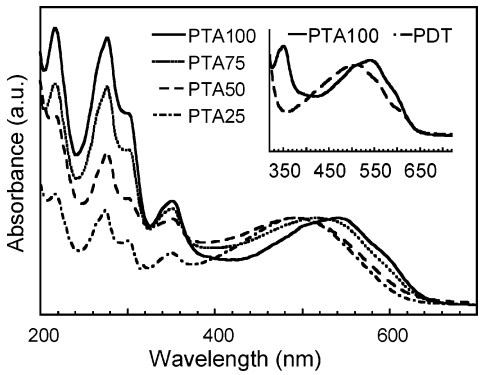

Figure 1. UV−vis absorption spectra of the PTA films. The absorptions of PTA100 and PDT are compared in the inset.

The LESR samples were prepared by filling a quartz ESR-grade tube with thick polymer films obtained by drop casting onto a plastic substrate; the ESR tubes were sealed under helium atmosphere. LESR was measured with a Bruker EMX spectrometer (X band), with a cryostat that controls the temperature between 4 and 40 K. The samples were excited with an Ar^+ laser line excitation at 459 nm through an optical fiber that terminates at the quartz tube inside the cavity. A microwave power of 20 μW was used for all measurements. g values were determined using a Bruker weak pitch sample to calibrate the spectrometer. The samples were cooled in the dark, and after each measurement, annealing to room temperature was performed to ensure the complete recombination of the previously excited carriers. The decay of the LESR signal was detected for 1 h after the illumination had been turned on for 5 min and then turned off.

Results and Discussion

(a) Electronic and Structural Characterization. The UV−vis absorption spectra of the copolymers films are reported in Figure 1. The spectra display an absorption band in the visible region that is due to the $\pi-\pi^*$ transition of the polythiophene backbone and a series of bands in the UV region that originates from the anthraquinone moieties.[26] The absorption band of the thiophene backbone is affected by the copolymer composition. A red shift is observed upon increasing the anthraquinone content, suggesting that these substituents are inducing a better conjugation and/or a better three-dimensional organization of the copolymer chains. The homopolymer PTA100 displays the most red-shifted spectrum, with λ_{max} at 540 nm. This feature can be reasonably ascribed to a better order because of the homogeneity of the side chains. It can be seen from the inset that PDT has a spectrum slightly blue-shifted with respect to PTA100, with λ_{max} at 510 nm. Considering that the two homopolymers have similar degrees of regioregularity, this is an indication that the anthraquinone molecules play a specific role in driving the chain ordering. In fact, in a previous paper, we studied the degree of order of PTAs by X-ray diffraction, finding that anthraquinone substituents induce a long-range lamellar organization of these polymer films, with a low extent of interlamellar stacking.[24] Thus, it seems likely that the observed red shift of the homopolymer absorption spectrum is not ascribable to interchain interaction but rather to a better

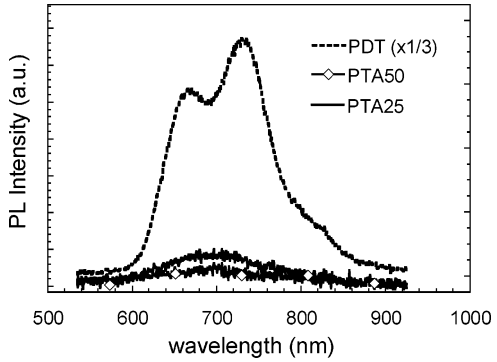

Figure 2. Photoluminescence spectra of PDT, PTA50, and PTA25 films at room temperature under a vacuum. The film thicknesses of the different polymers have been adjusted to obtain similar absorbances at the excitation wavelength (OD of 0.18 at 480 nm).

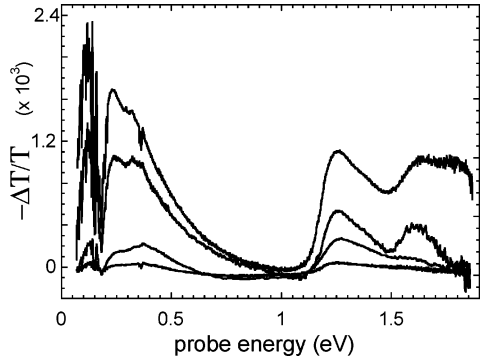

Figure 3. FTIR PA spectra of the PTAs. From bottom to top: PTA25, PTA50, PTA75, and PTA100. Temperature, 80 K; excitation wavelength, 514 nm; laser intensity, 1.75 mW/cm^2; shutter on/off modulation frequency, 0.21 Hz.

conjugation arising from some planarization of the thiophene backbone induced by the formation of domains of anthraquinone units of neighboring side chains, probably organized to some degree into columnar or layered structures.

It is interesting to note that thiophene-based copolymers containing acceptors such as fullerenes[18,19] have an opposite behavior with respect to PTAs. In this case, the π-electron delocalization of the conjugated backbone is preserved at low content of acceptor units,[19] but it is severely perturbed when the fullerene content is increased.[18] The flat geometry of anthraquinones has a lower steric hindrance compared to the spherical shape of fullerenes and is responsible for the specific role of this acceptor substituent in driving the chain ordering.

(b) Photoinduced Charge Transfer. The photoluminescence (PL) spectra of PTA films are compared to PDT in Figure 2. The PL is quenched with respect to PDT, and the quenching increases with the anthraquinone content. The quenching suggests that electron transfer from the photoexcited polythiophene backbone to anthraquinone is occurring and that the charge transfer is fast enough to compete with the radiative recombination of the excitons. In principle, energy transfer from the polymer to the acceptor can also lead to PL quenching. Because the anthraquinone electronic transitions are at higher energies with respect to the $\pi-\pi^*$ transition of the conjugated backbone (unlike other systems containing fullerenes or perylenes acceptors), energy transfer is ruled out as a possible step of the relaxation pathway.

The PA spectra of the PTAs (see Figure 3) display four broad bands related to electronic transitions and a series of infrared-active vibrations (IRAV bands) superimposed on the lower-energy band, which are indicative for the presence of charged photoexcitations.

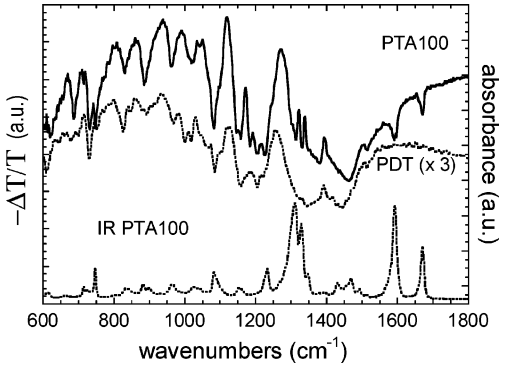

Figure 4. IRAV PA bands of PTA100 and PDT (magnified by 3) together with the IR absorbance of PTA100. Temperature, 80 K; excitation wavelength, 514 nm; laser intensity, 1.75 mW/cm^2; shutter on/off modulation frequency, 0.21 Hz.

To discern the origin of the PA features of PTAs, it is useful to compare them with PDT. Figure 4 displays the MIR region of the PA spectra of PTA100 and PDT, together with the IR absorbance of PTA100; for the sake of clarity, the other PTA spectra are omitted from the figure. It can be seen that the IRAVs of the PTAs have a spectral pattern similar to that of polyalkylthiophenes, thus probing the formation of charged polaronic excitations in the polythiophene backbone. There are, however, some extra features at 1589, 1668, and around 1330 cm^{-1}, whose spectral weight increases with the anthraquinone content. It is apparent that these features correspond to bleached IR absorption bands mainly arising from anthraquinone vibrational modes. The band at 1668 cm^{-1} is assigned to a C═O stretching, and the 1589, 1327, and 1308 cm^{-1} bands have mostly ring-stretching character.[27] Since spectroelectrochemical studies[26,28] indicate that the reduction of the antraquinone to a radical monoanion leads to the bleaching of these modes, we can reasonably presume that the spectral signatures of anthraquinone radical anions are observable in these PA spectra. In principle, two new positive bands, at 1500 and 1390 cm^{-1}, should also appear in the spectra,[26,28] but these effects are probably masked by the superposition of more intense polythiophene IRAV modes, considering that PA bands at these wavenumbers can also be seen in PDT. Therefore, we can conclude that the vibrational part of the PA spectra provides the spectroscopic fingerprint of long-lived metastable polaron cations in the polythiophene backbone and radical anions in the anthraquinone moieties, arising from the photoinduced charge-transfer process.

Further spectroscopic evidence for the photoinduced charge generation is given by the LESR measurements reported in Figure 5. The spectra display two overlapping lines at magnetic fields of ∼3361 and ∼3365 G corresponding to $g = 2.0042$ and $g = 2.0024$, respectively. The high-g-value signal is assigned to radical anions on the anthraquinone molecule,[29] and the low-g-value signal corresponds to positive polarons on the polythiophene chain.[30] Microwave saturation studies show different relaxation times for these spins, giving clear evidence of independent photoinduced spins.[8] The number of photogenerated spins increases with the content of anthraquinone acceptors in the copolymers.

The increased number of charges, due to the charge-transfer process, is also responsible for the enhancement of the PA signal with the anthraquinone content (see Figure 3). As we will discuss later, longer lifetimes are also responsible for this feature.

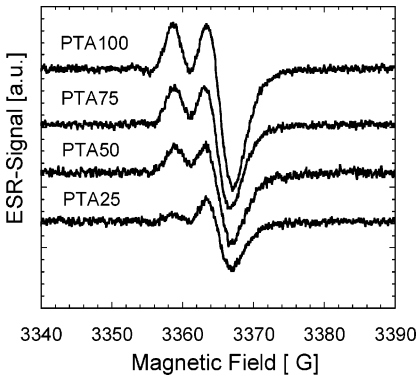

Figure 5. LESR spectra of the PTAs. Measurements were performed at a temperature of 20 K and a microwave power of 20 μW. The spectra shown are corrected for the weak dark signal and shifted along the *y* axis.

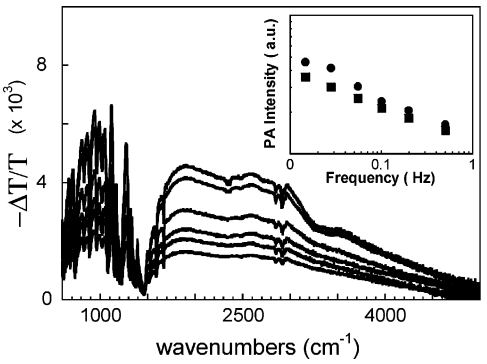

Figure 6. FTIR PA spectra of PTA100 obtained at different laser on/off modulation frequencies; from bottom to top, the shutter modulation frequencies are 0.5, 0.1, 0.055, 0.0286, 0.0147, and 0.0071 Hz, respectively. Temperature, 80 K; excitation wavelength, 514 nm; laser intensity, 3.5 mW/cm^2. Inset: PA intensity versus shutter modulation frequency for PTA100 (●) and PTA75 (■).

Another interesting aspect of the PA spectra of the copolymer series is that the spectral weights of the lower-energy and higher-energy electronic transitions increase with the anthraquinone content. The first question to answer is whether some of these transitions arise, as in the vibrational part, from the anthraquinone radical anions. Considering that the anthraquinone monoanion has three main transitions peaked in the UV−vis region, i.e., outside the MIR−NIR region probed by our experiments, plus a weak and broad transition smeared from 750 to 1050 nm,[26] it is conceivable that the observed PA transitions originate from the polythiophene backbone rather than from the anthraquinone charged photoexcitations.

In principle, one of the two bands observed above 1 eV might be due to neutral excitations of the conjugated backbone, as the steady-state PA spectra of polyalkylthiophenes display a band due to triplet excitations in this region. This type of assignment is quite unlikely in PTAs because we expect that the triplet population should be drastically reduced by the photoinduced charge transfer to anthraquinone. Therefore, we can reasonably infer that the observed transitions are due to the formation of polythiophene charged excitations rather than to triplet states. Considering that the spectral signature of polarons in polythiophenes consists of two bands,[31] one in the MIR region and one in the NIR region, it is conceivable that the four spectral features displayed in Figure 3 might arise from two coexisting charged photoexcitations whose relative concentration changes with the anthraquinone content. Since the anthraquinone substituents affect the three-dimensional order, these two photoexcitations might correspond to different structural organizations of the polymers. It is apparent from Figure 3 that the lower- and higher-energy bands increase their spectral weight with the amount of anthraquinone substituents. In highly ordered regioregular polyalkylthiophenes, two similar transitions have been assigned to the crystalline phase and to 2D polarons spread on different lamellae.[32] However, in PTAs, the type of order is quite different from that observed in highly crystalline polyalkylthiophenes. In PTA100 and PTA75, there is long-range lamellar organization, with good π-electron delocalization in the conjugated backbone, but rather poor interlamellar stacking.[24] For this reason, the formation of 2D polarons seems quite unlikely in these polymers.

In conclusion, the electronic PA spectra of the PTAs exhibit a change in shape with the content of acceptor substituents that, at least for the MIR region, seems to be related to changes in the chain conjugation induced by the anthraquinones. It is worth noting that, in general, the interpretation of the electronic part of the PA spectra of conjugated polymers is not straightforward, and the arguments regarding the assignments are often indirect. A typical approach used to discern the origin of the PA transitions is to probe the recombination mechanism of the various bands by studying their dependence on the photomodulation frequency and on the laser pump intensity. However, these types of measurements are not significant in PTAs because these polymers exhibit persistent charges whose population is affected by the thermal and illumination history. As discussed in the following section, the recombination mechanism can be better followed in the time domain, after a complete relaxation by thermal annealing.

(c) Kinetics of the Photoinduced Charges. Figure 6 displays the MIR PA spectra of PTA100 obtained at 80 K at different shutter on−off modulation frequencies. It can be seen that the steady-state condition is not fulfilled, as the PA intensity is reduced by increasing the shutter frequency. A similar effect is observed for PTA75 (see Figure 6 inset), whereas for PTA25 and PTA50, the PA signal is invariant with the shutter modulation frequency. Considering our experimental conditions, this indicates that the recombination of the photogenerated charged states occurs within 1 s when fewer than 50% of the thiophene are carrying an acceptor molecule and that lifetimes can be longer than 10 s when more than 50% of the thiophene are carrying an acceptor molecule. By increasing the temperature above 200 K, the recombination gets faster, and the PA spectra of PTA75 and PTA100 are unaffected by the modulation frequency.

The quite long lifetimes allow the use of our experimental setup to study the kinetics of the photogenerated charges in the time domain; the experimental reproducibility is good enough to perform the measurements in the MIR region but not in the NIR region. Figure 7 shows the PA spectra of PTA100 under constant illumination, recorded at various time delays from the switching on of the laser excitation. The signal exhibits a prompt increase in the first few seconds and then saturates, reaching a plateau after a delay on the order of 20 s. The spectral pattern is similar to that obtained with the on/off laser modulation technique, but the signal is 1 order of magnitude more intense. The rise of the PA intensity versus time, together with the decay after switching off the laser excitation, is depicted in the inset of Figure 7. The signal does not decay completely, indicating that persistent charges are formed upon photoexcitation; their recombination is favored by raising the temperature above 200 K. The decay features are not adequately reproducible, because of the long delays between the reference and the sample scan

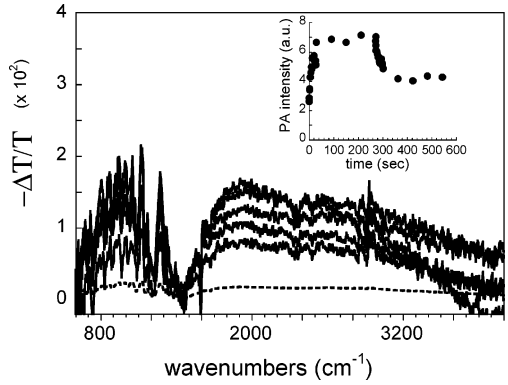

Figure 7. One-scan FTIR PA spectra of PTA100 recorded at various time delays from the turning on of the laser excitation (continuous lines); from bottom to top, the time delays are 0.93, 1.85, 6.56, 23, and 90 s, respectively. PA spectra obtained with the shutter on/off modulation of 0.21 Hz (dotted line). Inset: Rise and decay of the PA signal versus time. Temperature, 80 K; excitation wavelength, 514 nm; laser intensity, 3.5 mW/cm^2.

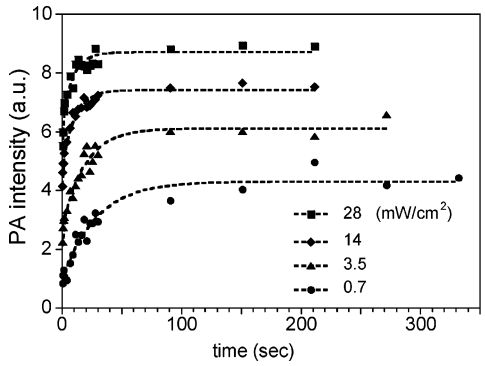

Figure 8. Rise of the PA intensity versus time for PTA100 at various laser pump intensities. Temperature, 80 K; excitation wavelength, 514 nm. Dotted lines, best fit; parameters listed in Table 1.

(more than 3 min). Therefore, we focused our kinetic studies on the rise of the PA signal versus time.

The rise of the PA signal of the homopolymer PTA100 is displayed in Figure 8 for four different laser intensities *I*. After the laser is switched on, the PA signal rises with time, reaching a plateau when the steady-state population of charged photoexcitations is achieved. Saturation effects with the laser intensity are observed: the plateau scales sublinearly with the laser intensity with an $I^{0.16}$ dependence, and the rise time decreases with increasing laser intensity. These features might be the result of defect-limited recombination processes in which the detected long-lived photoexcitations are assumed to be bound to traps and, as the pump intensity increases, the traps are filled, thus reducing the generation efficiency. A rate equation to include saturation effects has been proposed elsewhere as[33]

$$dN/dt = g - k^*N \quad (1)$$

where N is the photoexcitation density, proportional to the PA signal; k^* is an effective recombination rate coefficient, given by $(1/\tau + g/N_0)$ for monomolecular kinetics or $N[b + (g/N_0)^2]$ for bimolecular kinetics. Here, g is the bare generation rate, which is proportional to I, and N_0 is the trap density. The above rate equations describe both the observed saturation of the steady-state population and the faster rise when the laser intensity is increased. However the analytical solutions of eq 1 (for both mono- and bimolecular recombination) fit badly the PA rises displayed in Figure 8. The assumption, implicit in eq 1, is of a single recombination rate. As we have previously discussed, persistent charges with long relaxation times are observed in PTA100 and PTA75, and thus, a distribution of recombination rates should be considered. Similarly to other conjugated polymers and in analogy to amorphous and glassy materials,[34] it is possible to account for the distribution of the recombination times by adding a recombination rate coefficient k that has the following time dependence: $k \sim t^{m-1}$, where $0 < m < 1$. With much better fitting results, we used a simplified picture where just two effective relaxations are considered, a "fast" component that reaches the steady-state population (n_1) in shorter times than our ∼0.4 s time resolution and a "slow" component (n_2, τ_2) that, for simplicity, recombines monomolecularly: $N(t) = n_1 + n_2[1 - \exp(-t/\tau_2)]$. The fitting parameters are listed in Table 1. The "fast" component n_1 scales as $I^{0.49}$. The slow component n_2 does not vary significantly; just a slight decrease with the laser intensity is observed. On the other side, τ_2 decreases with I ($\tau_2 \sim I^{-0.43}$).

TABLE 1: Fitting Parameters Obtained from the PA Rise versus Time at Various Laser Intensities *I* for PTA100 (See Figure 8)[a]

laser intensity[b] (mW/cm^2)	n_1 (au)	n_2 (au)	τ_2 (s)
0.7	0.934	3.36	28.07
3.5	2.477	3.60	16.894
14	4.453	2.88	8.2167
28	5.77	2.79	5.7871

[a] PA: $N(t) = n_1 + n_2[1 - \exp(-t/\tau_2)]$. [b] $\lambda_{exc} = 514$ nm.

The recombination kinetics of the photogenerated charges was also studied by monitoring the decay of the LESR signal. Figure 9 displays the decay of the photogenerated spins of the PTAs at 20 K in darkness after 1 h of continuous illumination. The magnetic field was set to the high-field minimum (3367 G, Figure 7), i.e., in a region where the polaron P+ signal is dominant. The zero signal corresponds to the dark spin density, and the signal was normalized to the steady-state value that was reached after 1 h of illumination. The decay features are similar to those detected at low magnetic field, where the anthraquinone radical anion signal is dominant. This indicates that the recombination occurs mainly between radical pairs.

It can be seen in Figure 9 that, after the illumination is stopped, a rapid decay of the photogenerated spins is followed by a much slower component, associated with persistent charges that can still be observed after several minutes and even hours. The LESR decay does not vary with temperature below 40 K, but at higher temperatures, a steeper decay is observed, indicating some thermal detrapping and recombination of persistent charges. At 100 K, there are still a significant number of trapped spins that persist for several minutes; they disappear completely upon annealing of the sample to room temperature. Note that the persistent charges are detected in the whole PTA series.

The PA rise and LESR decay of the PTAs can be rationalized using a simple picture inspired by a model that was proposed to explain photoconductivity at low temperatures in amorphous inorganic semiconductors[10] and that has already been successfully used to explain the recombination mechanism of photogenerated spins in polymer/fullerene blends. Within this picture, the charges are photogenerated as radical cation and radical anion pairs, arising from the photoinduced electron transfer from the polymer backbone to anthraquinone. The vast majority of these pairs are bound by Coulomb attraction into geminate pairs that have a fast recombination. However, a fraction of them are separated into noninteracting charges, and even though the mobility of these charges is low (especially for radical anions on isolated acceptor molecules), they can still undergo some

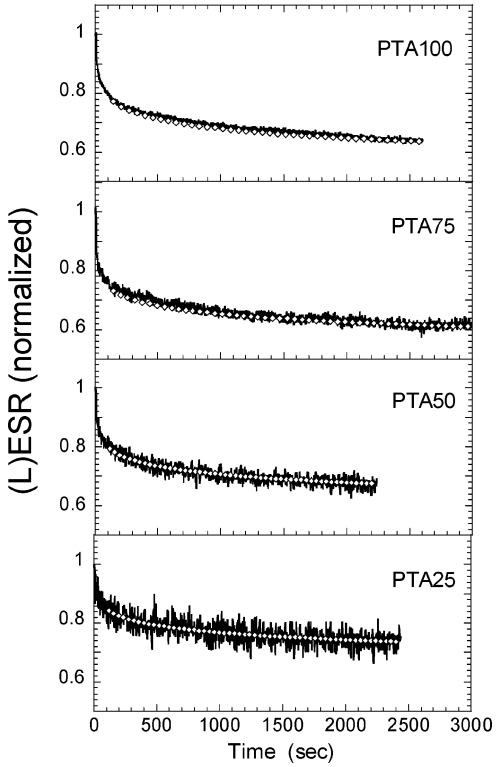

Figure 9. LESR decay of PTAs versus time, recorded at the LESR minimum (B = 3367 G). Temperature, 20 K; microwave power, 20 μW; laser excitation wavelength, 459 nm; laser intensity, 50 mW/cm^2. Open dotted line, best fit with eq 3; parameters listed in Table 2.

migration. Because of the structural and energetic disorder of conjugated polymers, before annihilation, the radical cations can be trapped into localized states, corresponding to chain segments with longer conjugation.[35]

When the laser is switched on, the generation and annihilation of the radical pairs start to occur. At shorter times, it is more likely that the photogenerated radical pairs will recombine geminately, whereas at longer times, nongeminate recombination prevails. As time elapses, the chance for a radical to be trapped into a localized state increases, and because the temperature is low, the detrapping by thermal excitation is less likely. The annihilation of the isolated trapped radicals occurs by tunneling or by recombination with a mobile radical that passes nearby.

The fast and slow components of the PA rise, presented in Table 1 and Figure 8, acquire a physical meaning within this framework: the fast component is due to radicals that recombine geminately or to mobile charges that find an oppositely charged radical to recombine, and the slow component corresponds to isolated trapped charges that are formed from the fast recombining population as time elapses. The dependence on the laser intensity of the lifetime (τ_2) and steady-state population (n_2) of the slow component is rationalized by the proposed scenario, having in mind that the laser intensity is varying the number of photogenerated carriers. The chance for a trapped charge to find an oppositely charged radical to annihilate is low when the number of photogenerated radical pairs is low, but it increases significantly for higher charge densities. Therefore, τ_2 is much longer at low laser intensities than at higher intensities. The photogenerated carrier density should not affect the steady-state population of the trapped charges, but should strongly influence the time necessary to reach the steady-state conditions. For this reason, n_2 is substantially not affected by the laser intensity.

The observed sublinear $I^{0.49}$ dependence of the fast recombining charge population might be due to bimolecular recombination of pairs that escaped geminate recombination and that are not yet trapped into localized states or to saturation effects arising from the formation of the trapped charges (the slow component).

It is interesting to note that the proposed scenario is consistent with the fact that long-lived trapped charges are not observed in the PA measurements of the copolymers with fewer than 50% of the thiophene moieties carrying an acceptor molecule. The density of radical pairs generated by the photon absorption is lower for lower contents of acceptors, and thus, the recombination lifetimes of the trapped charges (2−30 s in PTA100) should be several minutes for PTA25 and PTA50. As our experimental setup probes only metastable excitations that recombine within less than 1 min, the persistent trapped charges of PTA25 and PTA50 have recombination times that are too long to be detected in the PA measurements.

In polymer/fullerene blends, the presence of trapped spins at low temperatures has been already observed.[8,9] The decay of the LESR signal in these donor/acceptor systems has been successfully fitted using a model developed by Dunstan to describe the distant electron−hole pair recombination at low temperatures in amorphous silicon.[9] The same type of model is used here to fit the LESR decays of PTAs. The model describes the recombination of the residual trapped carriers that survive fast geminate recombination; thermal reexcitation of the trapped carriers is neglected. The details of the model have been developed elsewhere,[10] but the basic assumptions are substantially as follows:

(a) Spatially close carriers have much higher recombination rate than distant carriers

$$\nu(R) = \nu_0 \exp\left(-\frac{2R}{a}\right) \tag{2}$$

where $\nu(R)$ describes the recombination rate of any electron and hole that are separated by a distance R, $\nu_0 = \tau_0^{-1}$ is a recombination rate constant that depends on the energy, and the parameter a is an effective localization radius.

(b) Charge neutrality holds in the system, i.e., the density of trapped electrons is the same as the density of trapped holes.

The residual spin carrier concentration $n(t)$, for times long enough to assume that solely nongeminate recombination is occurring, follows the equation

$$\frac{n(t)}{n_0} = \frac{\frac{n_1}{n_0}}{1 + \left(\frac{n_1}{n_0}\right)\frac{\pi}{6} n_0 a^3 \left[\ln^3\left(\frac{t}{\tau_0}\right) - \ln^3\left(\frac{t_1}{\tau_0}\right)\right]} \tag{3}$$

where n_0 is the initial spin carrier concentration when the laser is turned off at time $t = 0$ and n_1 is the spin concentration at time $t = t_1$ where solely nongeminate recombination occurs. Because of uncertainties both in the sample volume that is illuminated and in the ESR technique, it is critical to determine the absolute concentration of the photoexcited spins from the LESR signal. For this reason, $n(t)$ was normalized to the steady-state concentration n_0, and eq 3 was used to fit the normalized LESR decays of PTAs displayed in Figure 9.

The fits were obtained choosing t_1 = 2 min to completely avoid geminate recombination; the values n_1/n_0 were obtained from the data, and only the product $n_0 a^3$ and the prefactor τ_0 entered as fit parameters. The data were satisfactorily fitted with a recombination time constant τ_0 of about 10^{-5}−10^{-6} s for the whole copolymer series. The values of $n_0 a^3$, obtained using a

TABLE 2: Fitting Parameter a^3n_0 Obtained from the LESR Decays of the Radical Cation Spins of the PTAs at 20 K, 50 mW/cm² (See Figure 9)[a]

polymer	weight fraction of acceptors (%)	number of acceptors/cm³ [b]	a^3n_0 [c]	n_0 spins/cm³ [d]
PTA25	16.8	4.9095×10^{17}	9×10^{-5}	2.6×10^{17}
PTA50	26.4	7.715×10^{17}	1.2×10^{-4}	3.5×10^{17}
PTA75	32.6	9.5278×10^{17}	1.4×10^{-4}	4.1×10^{17}
PTA100	36.9	10.783×10^{17}	1.5×10^{-4}	4.4×10^{17}

[a] Using eq 3. [b] Density of the PTAs is around 1 mg/cm³. [c] $\tau_0 = 1$ μs for every PTA. [d] Number of photogenerated radical cations estimated from a^3n_0, with $a = 7$ Å.

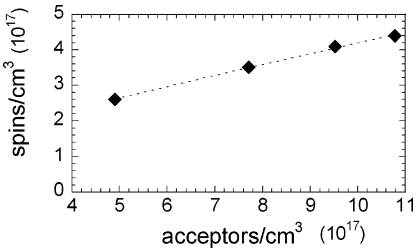

Figure 10. Density of the photogenerated cations as a function of the density of anthraquinone acceptor for the PTA films. An effective delocalization radius of 7 Å was assumed (see Table 2).

recombination time constant $\tau_0 = 1$ μs, are listed in Table 2. Similar values of τ_0 were also found in conjugated polymer/fullerene blends and have been related to the polaronic relaxation of the radical cation that determines an energy barrier to recombination and thus increases the recombination lifetime with respect to the much shorter recombination times in amorphous silicon.[9] As τ_0 depends on the recombination energy barrier and not on the number of photogenerated charges, it is reasonable to assume that τ_0 is not influenced by the copolymer composition. Note that τ_0 can be fixed with some discretion because of the weak dependence of $n(t)/n_0$ on τ_0 (eq 3): a variation within 1 order of magnitude induces changes in the other parameter n_0a^3 of only about 10%.

The parameter n_0a^3, listed in Table 2, shows an increase with increasing PTA acceptor content. These variations must be related to the density of the anthraquinone molecules n_A rather than to the copolymer composition, given in molar fractions (see Experimental Section). Therefore, n_A was calculated for each polymer using the molar fraction composition and the film densities measured by floating techniques (the densities were found be around 1 g/L for the whole PTA series).

It is apparent from Table 2 that n_0a^3 scales linearly with n_A. As already mentioned, it is critical to obtain n_0 directly from the LESR signal, but the values of n_0a^3 obtained from the fitting of the LESR decays can be used for this purpose if a rough evaluation of the extent of the effective localization radius a is provided (see Table 2 and Figure 10). We can expect that a should be longer than 5 Å and could be around 6−7 Å considering that (a) the photoexcited electrons are localized within the anthraquinone molecule, whose dimension is around 7 Å; (b) the positive charge in the thiophene backbone is delocalized within 4−5 monomeric units; and (c) the length of the alkylic segment between the thiophene and anthraquinone units is around 5 Å. Taking $a = 7$ Å, we find that $n_0 = 0.3n_A$; if a is reduced, n_0 increases, and the value $n_0 = n_A$ is reached for a localization radius of 4.7 Å.

We can thus conclude that the steady-state population of radical cations n_0, obtained from the fitting of the LESR decay with eq 3, scales linearly with the density of anthraquinone acceptors n_A. n_0 does not exceed n_A and is roughly of the same order of magnitude as the acceptor density. This brings support to the model proposed to describe the photoexcitation behavior as (i) n_0 cannot exceed n_A to fulfill charge neutrality requirements (see the basic assumptions of the model), and (ii) under our experimental conditions, the system is almost in the saturation regime, so that we indeed expect that n_0 should be of the same order of magnitude as n_A.

Conclusions

In this work, we present a detailed study of the photoinduced charge-transfer properties of a series of polyalkylthiophene copolymers carrying anthraquinone substituents covalently linked to the conjugated backbone. Photoinduced absorption (PA) and light-induced electron spin resonance (LESR) measurements indicate the formation of metastable charges arising from photoinduced electron transfer from the polythiophene backbone to the anthraquinone moieties.

The recombination kinetics of the metastable charges was studied at low temperatures, where persistent charges are observed. The results are successfully rationalized using a photoexcitation scenario, inspired by a theoretical model proposed to describe the photoconductivity at low temperatures in amorphous inorganic semiconductors. The model nicely fits the LESR decays and is consistent with the kinetics features of the photoinduced absorption. The observed trapped charges are intrinsic to the donor/acceptor system, being the result of charge separation. By studying their recombination, a coherent photophysical picture is provided, where the key role played by the number of acceptor substituents, tuned by chemical tailoring, is nicely evidenced.

Around room temperature, i.e., near the operating device conditions, faster recombination will occur. The photophysical study presented in this work suggests that long-lived metastable charges are also formed at room temperature. In future studies, faster time-resolved spectroscopies will be useful for monitoring these aspects.

Based on the long photoinduced charge separation and the advantageous solution properties, these copolymeric conjugated polymer/anthraquinone systems may lead to interesting applications in optoelectronic devices in the near future.

Acknowledgment. Financial support from the European Commission (EUROMAP RTN Project HPRN-CT-2000-00127), from the Italian Ministry of Research and Education (MIUR-FIRB RBNE03SXZ Synergy project), and from the Cariplo Foundation (PROTEO project) is gratefully acknowledged.

References and Notes

(1) Brabec, C. J.; Sariciftci, N. S.; Hummelen, J. C. *Adv. Funct. Mater.* **2001**, *11*, 15.
(2) Nelson, J. *Curr. Op. Solid State Mater. Sci.* **2002**, *6*, 87.
(3) Sariciftci, N. S.; Smilowitz, L.; Heeger, A. J.; Wudl, F. *Science* **1992**, *258*, 1474.
(4) Morita, S.; Zakhidov, A. A.; Yoshino, K. *Solid State Commun.* **1992**, *82*, 249.
(5) Brabec, C. J.; Zerza, G.; N. Sariciftci, S.; Cerullo, G.; De Silvestri, S.; Luzzati, S.; Hummelen, J. C. *Chem. Phys. Lett.* **2001**, *340*, 232.
(6) Kraabel, B.; Lee, C. H.; McBranch, D.; Moses, D.; N. Sariciftci, S.; Heeger, A. J. *Chem. Phys. Lett.* **1993**, *213*, 389.
(7) Smilowitz, L.; Sariciftci, N. S.; Wu, R.; Gettinger, C.; Heeger, A. J.; Wudl, F. *Phys. Rev. B* **1993**, *47*, 13835.
(8) Dyakonov, V.; Zoriants, G.; Scharber, M.; Brabec, C. J.; Janssen, R. A.; Hummelen, J. C.; Sariciftci, N. S. *Phys. Rev. B* **1999**, *59*, 8019.
(9) Schultz, N. A.; Scharber, M. C.; Brabec, C. J.; Sariciftci, N. S. *Phys. Rev. B* **2001**, *64*, 245219.
(10) Yan, B.; Schultz, N.; Efros, A. L.; Taylor, P. C. *Phys. Rev. Lett.* **2000**, *84*, 4180.

(11) Yu, G.; Gao, J.; Hummelen, J. C.; Wudl, F.; Heeger, A. J. *Science* **1995**, *270*, 1789.
(12) Hall, J. J. M.; Walsh, C. A.; Greenham, M. C.; Marseglia, E. A.; Friend, R. H.; Moratti, S. C.; Holmes, A. B. *Nature* **1995**, *376*, 498.
(13) Shaheen, S. A.; Brabec, C. J.; Padinger, F.; Fromherz, T.; Hummelen, J. C.; Sariciftci, N. S. *Appl Phys. Lett.* **2001**, *78*, 841.
(14) Stalmach, U.; de Boer, B.; Videlot, C.; van Hutten, P. F.; Hadziioannou, G. *J. Am. Chem. Soc*. **2000**, *122*, 5464.
(15) Neuteboom, E. E.; Meskers, S. C. J.; van Hal, P. A.; van Duren, J. K. J.; Meijer, E. W.; Janssen, R. A. J.; Dupin, H.; Pourtois, G.; Cornil, J.; Lazzaroni, R.; Brédas, J.-L.; Beljonne, D. *J. Am. Chem. Soc*. **2003**, *125*, 8625.
(16) Cravino, A.; Sariciftci, N. S. *J. Mater. Chem.* **2002**, *12*, 1931.
(17) Ramos, M.; Rispens, M. T.; van Duren, J. K. J.; Hummelen, J. C.; Janssen, R. A. J. *J. Am. Chem. Soc.* **2001**, *123*, 6714.
(18) Cravino, A.; Zerza, G.; Neugebauer, H.; Maggini, M.; Bucella, S.; Menna, E.; Svensson, M.; Andersson, M. R.; Brabec, C. J.; Sariciftci, N. S. *J. Phys. Chem. A* **2002**, *106*, 70.
(19) Zhang, F.; Svensson, M.; Andersson, M. R.; Maggini, M.; Bucella, S.; Menna, E.; Inganäs, O. *Adv. Mater.* **2001**, *13*, 171.
(20) Zerza, G.; Cravino, A.; Neugebauer, H.; N. Sariciftci, S.; Gómez, R.; Segura, J. L.; Martín, N.; Svensson, M.; Andersson, M. R. *J. Phys. Chem. A* **2001**, *105*, 4172.
(21) Giacalone, F. J.; Segura, L.; Martín, N.; Catellani, M.; Luzzati, S.; Lupsac, N. *Org. Lett.* **2003**, *5*, 1670.
(22) Russel, D. M.; Arias, A. C.; Friend, R. H.; Silva, C.; Ego, C.; Grimsdale, A.; Müllen, K. *Appl. Phys. Lett.* **2002**, *80*, 2204.
(23) Martinez-Diaz, M. V.; Esperanza, S.; de la Escosura, A.; Catellani, M.; Yunus, S.; Luzzati, S.; Torres, T. *Tetrahedron Lett.* **2003**, *44*, 8475.
(24) Catellani, M.; Luzzati, S.; Lupsac, N. O.; Mendichi, R.; Consonni, R.; Famulari, A.; Meille, S. V.; Giacalone, F.; Segura, J. L.; Martin, N. *J. Mater. Chem.* **2004**, *14*, 67.
(25) Luzzati, S.; Scharber, M.; Catellani, M.; Lupsac, N.; Giacalone, F.; Segura, J. L.; Martin, N.; Neugebauer, H.; Sariciftci, N. S. *Synth. Met.* **2003**, *139*, 731.
(26) Büschel, M.; Stalder, C.; Lambert, C.; Beck, M.; Daub, J. *J. Electroanal. Chem.* **2000**, *484*, 24.
(27) Pecile, C.; Lunelli, B. *J. Chem. Phys.* **1967**, *46*, 2109.
(28) Juchnovski, I.; Kolev, T. *Spectrosc. Lett.* **1986**, *19*, 1181.
(29) Vuolle, M.; Mäkelä, R. *J. Chem. Soc., Faraday Trans.* **1987**, *183*, 51.
(30) Zerza, G.; Cravino, A.; Neugebauer, H.; Sariciftci, N. S.; Gómez, R.; Segura, J. L.; Martin, N.; Svensson, M.; Andersson, M. R. *J. Phys. Chem. A* **2001**, *105*, 4172.
(31) Lane, P. A.; Wei, X.; Vardeny, Z. V. *Phys. Rev. Lett.* **1996**, *77*, 1544.
(32) Österbacka, R.; An, C. P.; Jiang, X. M.; Vardeny, Z. V. *Science* **2000**, *287*, 839.
(33) Ehrenfreund, E.; Epshtein, O.; Eichen, Y.; Wohlgenannt, M.; Vardeny, Z. V. *Synth. Met.* **2003**, *137*, 1363.
(34) Epshtein, O.; Nakhmanovich, G.; Eichen, Y.; Ehrenfreund, E. *Phys. Rev. B* **2001**, *63*, 125206.
(35) Rauscher, U.; Schütz, L.; Greiner, A.; Bässler, H. *J. Phys.: Condens. Matter* **1989**, *1*, 9751.